

Photon polarisation in light-by-light scattering: finite size effects

Victor Dinu,^{1,*} Tom Heinzl,^{2,†} Anton Ilderton,^{3,‡} Mattias Marklund,^{3,§} and Greger Torgrimsson^{3,¶}

¹*Department of Physics, University of Bucharest, P. O. Box MG-11, Măgurele 077125, Romania*

²*School of Computing and Mathematics, Plymouth University, Plymouth PL4 8AA, UK*

³*Department of Applied Physics, Chalmers University of Technology, SE-41296 Gothenburg, Sweden*

We derive a simple expression for the photon helicity and polarisation-flip probabilities in arbitrary background fields, in the low energy regime. Taking the background to model a focused laser, we study the impact of pulse shape and collision geometry on the probabilities and on ellipticity signals of vacuum birefringence. We find that models which do not account for pulse duration can overestimate all signals by an order of magnitude. Taking pulse duration into account, the flip probability becomes relatively insensitive to both angular incidence and the fine details of the pulse structure.

I. INTRODUCTION

It has been known since the early days of quantum electrodynamics (QED) that the appearance of virtual pairs leads to nonlinearities, due to the possibility of light-by-light scattering [1–3]. These nonlinearities can manifest as effects akin to those in nonlinear optics [4]: for example, a macroscopic, classical light source of sufficiently high intensity can alter the polarisation state of probe photons, leading to ‘vacuum’ birefringence [5]. (Note that ‘vacuum’ here highlights only the absence of matter.)

In [6] a proposal was made to demonstrate these nonlinearities. Because the birefringence effect increases with (target) field strength and probe frequency, it was suggested to use an intense, high-power laser as a target (implying a gain in field strength of many orders of magnitude compared to experiments using magnets [7, 8]) and an X-ray free electron laser (XFEL) as a probe. This scenario will be realised with the HIBEF facility employing the European XFEL at DESY [9]. Even higher intensities and probe energies will be achieved after the completion of the Extreme Light Infrastructure nuclear physics pillar (ELI-NP) [10]. The search for vacuum birefringence at HIBEF has been selected as its flagship experiment. It thus seems timely to extend the results of [6] by considering more realistic background field distributions modelling focused, pulsed lasers. This will also provide some theoretical underpinning for a detailed experimental feasibility study that is currently under way [11].

To further motivate our investigation, recall that a beam of light, wavelength λ' , probing a birefringent medium acquires an ellipticity δ in its polarisation. In optics, δ can be expressed in terms of the refractive indices $\{n_{\perp}, n_{\parallel}\}$ of the medium, and the distance d travelled in the medium by the probe as $\delta = \pi d(n_{\perp} - n_{\parallel})/\lambda'$. This expression also holds for vacuum birefringence, under the

assumptions that 1) this is induced by a homogenous, constant field, and 2) the probe is a plane wave. However, the targets and probes in upcoming experiments are lasers, and all fields will be focused, pulsed, and varying in space and time. Because the ellipticity is small and will be challenging to measure, a comprehensive discussion of potential experiments requires more careful modelling of the target and probe (as well as an analysis of background noise, losses in polarisers and lenses, and so on [11]). As a step toward this goal, it would be useful to have some simple estimates of various effects. The purpose of this paper is, in part, to give such formulae covering the case of beam geometry, in order to understand the impact of pulse shape and duration.

As stated above, and emphasised in [12], vacuum birefringence is a manifestation of photon-photon scattering. Hence, a measurement of the former would represent the first observation of the latter in a set-up with *all* photons involved being real (unlike, say, in Delbrück scattering [13, 14]). For real photon-photon scattering there are currently only upper bounds on the cross section [15]. The QED scattering processes underlying vacuum birefringence are therefore of interest [16, 17], and it is natural to take an S -matrix approach to this topic. This was the approach taken in [12], in which we showed that the most relevant process is that in which probe photons flip between orthogonal helicity or polarisation states when passing through the background field. For the analytically solvable case of plane wave targets and probes, we obtained the helicity flip probability and the resulting probe ellipticity for arbitrary energies and intensities. The second purpose of this paper is to extend those results to cover backgrounds describing focused laser pulses in the relevant parameter regime. In the future we will also include the probe geometry, but here we take a more modest step by studying the flip probability for photons probing intense, focused laser fields.

The paper is organised as follows. In Section II we derive the flip probability from the QED S -matrix; it takes the form of a simple integral over the worldline of a massless particle. In Section III we use this to model the impact of field and collision geometries on the flip probability, and describe the implications for detecting signals of vacuum birefringence. We conclude in Section IV.

* dinu@barutu.fizica.unibuc.ro

† theinzl@plymouth.ac.uk

‡ anton.ilderton@chalmers.se

§ mattias.marklund@chalmers.se

¶ greger.torgrimsson@chalmers.se

II. A WORLDLINE INTEGRAL FOR HELICITY AND POLARISATION FLIP

We begin with the probability for a photon, momentum l_μ , to flip helicity state $\epsilon_\mu \rightarrow \epsilon'_\mu$ when passing through a given background field $f_{\mu\nu}$. For the particular case of a plane wave background depending on nx with $n^2 = 0$, a direct QED calculation of the amplitude, to 1-loop order and exact in all other parameters, was given in [12]. In the low energy regime relevant to laser-based experiments, the scattering amplitude reduces to

$$T = \frac{\alpha}{30\pi} \frac{1}{E_S^2} \int \frac{d(nx)}{nl} (lf(x)\tilde{\epsilon}') (lf(x)\epsilon). \quad (1)$$

Our first task is to generalise this to arbitrary $f_{\mu\nu}$. To do so, recall first that a massless particle, momentum l_μ , follows a null geodesic in spacetime. In Minkowski space, any ‘lightfront time’ nx provides a suitable affine parameterisation of the geodesic, the explicit form of which is¹,

$$x_l^\mu(nx) = x^\mu(0) + \frac{l^\mu}{nl} nx \implies dx_l^\mu = \frac{l^\mu}{nl} d(nx). \quad (2)$$

Using this measure in (1) (extracting a factor of l_μ from the integrand turns the measure into dx_l^μ more explicitly) and taking $f_{\mu\nu}$ to be arbitrary and evaluated on the path (2), gives us a candidate expression for the flip amplitude in arbitrary backgrounds. Remarkably, this worldline integral is the correct expression, as we confirm below. Here we describe the physics it contains, beginning by writing it in a more revealing form.

The integral (1) also gives the amplitude for a photon to flip between *any* two orthogonal polarisation states with $\epsilon'\epsilon = 0$ (and $\epsilon^2 = \epsilon'^2 = -1$) not only helicity states [12]. We are interested in linearly polarised probes for birefringence, so we take $\{\epsilon, \epsilon'\}$ to be real; T is then real. Recall that it is possible to choose polarisation vectors which are orthogonal to both l_μ and a second light-like n_μ [18, 19], and so the vectors in play form a tetrad,

$$g_{\mu\nu} = \frac{n_\mu l_\nu + l_\mu n_\nu}{nl} - \epsilon_\mu \epsilon_\nu - \epsilon'_\mu \epsilon'_\nu. \quad (3)$$

Using this and the background energy-momentum tensor $\Theta_{\mu\nu} = f_{\mu\nu}^2 - g_{\mu\nu} \frac{1}{4} \text{tr} f^2$, we can rewrite (1) as

$$T = \frac{\alpha}{60\pi} \frac{1}{E_S^2} \int \frac{d(nx)}{nl} \left[l\Theta(x_l)l - (lf(x_l)\tilde{\epsilon})^2 \right], \quad (4)$$

with $\tilde{\epsilon} := \epsilon - \epsilon'$. The first term in the integrand of (4) is the null projection of the energy-momentum tensor as seen locally by the probe. It’s appearance is to be expected [20] and maximising it maximises the probability

¹ This parameterisation cannot be used if $n_\mu \propto l_\mu$, for then $ln = 0$; this is a manifestation of the zero mode problem of lightfront quantisation [18, 19]. In this case, the problem is avoided simply by choosing a different n_μ as parameter.

(since the amplitude is now real). The second term in (4) is negative, and therefore reduces the amplitude, but can be made to vanish for appropriate choices of collision and polarisation geometries. The combination $lf\epsilon$ which appears is typical of polarisation transport [21].

As it should be, (4) is reparameterisation invariant (most easily seen by extracting a factor of l_μ and writing the measure as dx_l^μ) and gauge invariant (shifting the polarisation vectors by l_μ does not affect amplitude). The integral is taken not over time, or position, but over the worldline of a massless particle, and so is fully relativistic. The form of (4) is similar to that of the eikonal found in high-energy scattering at small momentum transfer, which is also given by an integral over a classical particle trajectory, see [22, §9.1.1] or [23, §9.6]. Here the presence of a worldline (rather than spacetime) integral encodes the possibility that T vanishes when the photon misses a compactly supported background. The photon momentum l_μ is on-shell, underlining that we have abandoned the effective approach in favour of a ‘microscopic’ approach, and constant, because only the forward-scattering flip amplitude is relevant for birefringence. The reason why will be given below, when we derive (4) from the S -matrix. The reader primarily interested in phenomenology may proceed directly to Sect. III, where we evaluate the worldline integral.

A. Derivation from low-energy scattering in QED

To derive (1) from QED, we would first write down the one-loop S -matrix element for helicity flip in a background field, and integrate out the fermions (giving the polarisation tensor, see e.g. [24–28] and references therein). Though this cannot be done analytically for arbitrary backgrounds and arbitrary probe frequencies, we note that (1) is a low-energy approximation, of the same order as if we had treated the background perturbatively [29], and that there are no derivatives on the field. Therefore, given the approximations involved, it is simplest to begin with the low-energy Heisenberg-Euler effective action [2, 3], see e.g. [30, §5.1],

$$\mathcal{L}_{HE} = \frac{1}{4} \text{tr} F^2 + \frac{2\alpha^2}{45m^4} \left[\frac{7}{4} \text{tr} F^4 - \frac{5}{8} (\text{tr} F^2)^2 \right]. \quad (5)$$

We have written, for example, $\text{tr} F^2 = F^\mu{}_\nu F^\nu{}_\mu = -F^{\mu\nu} F_{\mu\nu}$ and we have used the formula [16]

$$(\text{tr} F \tilde{F})^2 = 4 \text{tr} F^4 - 2 (\text{tr} F^2)^2, \quad (6)$$

to remove the dual tensor. The background f is introduced by replacing $eF \rightarrow eF + ef$, and retaining only terms which are quadratic in both F and f (other terms do not contribute here).

We will calculate the probability for an incoming photon to scatter, momentum $p_\mu \rightarrow l'_\mu$, and flip polarisation, $\epsilon \rightarrow \epsilon'$ with $\epsilon'\epsilon = 0$. We begin with the S -matrix element,

which is obtained as usual from LSZ reduction of the correlation functions generated using the Lagrangian (5). It takes the form typical of scattering from an external, classical potential, in this case $f_{\mu\nu}^2$,

$$\langle l', \epsilon' | S | p, \epsilon \rangle = \int d^4x e^{i(l' - p)x} [F_{\text{in}} F_{\text{out}} f^2(x)], \quad (7)$$

in which x is the vertex position, $F_{\text{in}}^{\mu\nu} = p^{[\mu} \epsilon^{\nu]}$, $F_{\text{out}}^{\mu\nu} = l'^{[\mu} \epsilon'^{\nu]}$ and $[F_{\text{in}} F_{\text{out}} f^2]$ is shorthand for the (several) trace terms in $\mathcal{L}[F_{\text{in}} + F_{\text{out}} + f]$ which are quadratic in f and linear in F_{in} and F_{out} .

The states in (7) are, as normal, localised in momentum space. However, real probes are localised in both momentum and position. Probes can be narrower than background beams, and entirely miss them if not properly aligned. Neither of these situations can be described if the probe is taken to be a momentum eigenstate. Hence, localisation in position space becomes relevant, and we require a wavepacket for the probe. The full scattering amplitude to calculate is then

$$S_{fi} := \int d\mathbf{p} \psi(p) \langle l', \epsilon' | S | p, \epsilon \rangle, \quad (8)$$

in which $d\mathbf{p}$ is the Lorentz-invariant measure over the positive energy mass shell and the wavepacket ψ obeys

$$\psi(p) = \Lambda(p) e^{ipx_0} \quad \text{with} \quad \int d\mathbf{p} |\Lambda(p)|^2 = 1. \quad (9)$$

Here x_0 is the initial position about which the wavepacket is centred and $\Lambda(p)$ is sharply peaked (to be made precise below) around momentum $p_\mu = l_\mu$. The measure depends on three momentum coordinates, which can be ordinary vector momentum, but since we are dealing with photons it seems natural to take $\mathbf{p} = \{np, p^\perp\}$ defined with respect to some lightlike direction n_μ . This corresponds to a foliation of spacetime into a time nx and three spatial directions \mathbf{x} ; this will be of use below.

We first Fourier transform the background,

$$f_{\mu\nu}(x) = \int d^4k e^{-ikx} f_{\mu\nu}(k), \quad (10)$$

and perform the three \mathbf{x} -integrals in (8) (an integral over nx remains), giving three delta-functions. Because the external momenta are on-shell (three degrees of freedom), this is enough to determine a relation between the incoming and outgoing momenta; writing $\kappa = k + k'$, the sum of momenta coming from the two factors of $f_{\mu\nu}$, we find

$$p = l' - \kappa - \frac{(l' - \kappa)^2}{2n(l' - \kappa)} n. \quad (11)$$

For e.g. the HIBEF experiment, the typical background momentum ($|\mathbf{k}|$, optical) is much lower than the electron rest mass, and also much smaller than the typical probe momentum ($|\mathbf{l}|$, x-ray), so $|\mathbf{k}| \ll |\mathbf{l}|$. We want to evaluate S_{fi} under these assumptions. We therefore make a

low energy approximation typical when considering e.g. infra-red effects [31, 32]. In the exponent, we neglect quadratic (and higher) powers of the background momenta². Outside the exponent, we also expand to linear order in these momenta. Dropping $\{k, k'\}$ in the trace terms of (7) corresponds to neglecting derivative terms which have in any case been neglected in deriving (5); the result is that $F_{\mu\nu}^{\text{in}} \rightarrow l'_{[\mu} \epsilon_{\nu]}$ and $F_{\mu\nu}^{\text{out}} \rightarrow l'_{[\mu} \epsilon'_{\nu]}$. With this, the traces simplify considerably and we recover the structure in (1). Finally, to be able to neglect $\{k, k'\}$ in the wavepacket Λ we have to assume that

$$|(p - l') \partial_{l'} \Lambda(l')| \ll |\Lambda(l')|. \quad (12)$$

Since $p - l' = \mathcal{O}(k)$, (12) implies that the wavepacket cannot be too sharply peaked; its momentum space width Δ should be larger than the typical background momentum, $\Delta \gg |\mathbf{k}|$. What this means physically is that, in position space, the probe is localised at scales on which the background varies. This is seen explicitly by noting that, in the low energy approximation, (11) becomes

$$p = l' - \kappa + \frac{l' \kappa}{nl'} n, \quad (13)$$

so that when we undo the Fourier transformations (10), both $f_{\mu\nu}$ and the scattering amplitude become supported on a classical photon trajectory $x_{l'}^\mu$ as in (2):

$$\int d^4k f(k) \exp -ik \left(x_0 + \frac{l'}{nl'} n(x - x_0) \right) = f(x_{l'}). \quad (14)$$

A trivial reparameterisation trades x_0 for $x(0)$. The assumption that we can neglect k in the wavepacket has resulted in each of its modes being scattered forward³. Explicitly, the amplitude becomes $S_{fi} = \Lambda(l') T(x_{l'})$, which is the worldline integral (1), with path $x_{l'}^\mu$. The total probability of scattering with a polarisation flip is then

$$\mathbb{P}_{\text{flip}} = \int d\mathbf{l}' |S_{fi}|^2 = \int d\mathbf{l}' |\Lambda(l')|^2 |T(x_{l'})|^2. \quad (15)$$

If we further assume that the width of the wavepacket is small compared to the typical probe momentum ($\Delta \ll |\mathbf{l}|$) then we can as usual drop the wavepacket and integral from (15) and replace $l'_\mu \rightarrow l_\mu$, upon which the probability becomes

$$\mathbb{P}_{\text{flip}} = \mathbb{P}_{\text{forward+flip}} = |T(x_l)|^2. \quad (16)$$

² While all energies are low compared to m , the probe energy is *high* in comparison to that of the background, leading to low momentum transfer. Hence it is not so surprising that our amplitude has similarities to that in eikonal scattering.

³ We note in passing that for plane wave backgrounds one can take $n \propto k$, and (11) reduces to $p = l'$. The condition (12) is then satisfied automatically and the photon always scatters forward.

B. Quantum reflection

To arrive at (16) we assumed a separation of scales, namely that the characteristic frequency of the background is much smaller than that of the probe. It is interesting to ask what happens when this is not the case, and to compare with the quantum reflection calculation in [33]. Let the background now depend on a single spatial coordinate $x^1 \equiv x$. Three of the integrals in (7) can then be performed, giving a delta function supported on vector $\mathbf{p} = \{\pm l'_1, l'_2, l'_3\}$, describing forward (+) or back (-) scattering. Assuming the background polarisation is x -independent, the probabilities for forward scattering and reflection become, schematically,

$$\mathbb{P}_{\text{for.}} \propto \left| \int dx f^2(x) \right|^2, \quad \mathbb{P}_{\text{ref.}} \propto \left| \int dx e^{2il_1 x} f^2(x) \right|^2, \quad (17)$$

where the (different) proportionality constants depend on the probe momentum and polarisation, and the vector structure of the background. The reflection probability has the same structure as the reflection coefficient in [33], and will be much smaller than the forward scattering probability *unless* the background has support for momentum on the order of the probe momentum. Hence, for proposed ‘optical + xray’ laser experiments we expect photon reflection to be a small effect compared to birefringence. However, for other setups, as described in detail in [33], it would be easier to look for the reflection signal, which has the advantage of being more easily separated from experimental noise.

III. EXAMPLES IN GAUSSIAN BEAMS AND PULSES

In the remainder of this paper we evaluate the flip amplitude for photons in various collision geometries with backgrounds modelling intense laser fields. (For reviews of classical and quantum physics in strong laser fields see [34, 35].) The extension to beam-like probes will be considered elsewhere, but our results are still useful in the context of vacuum birefringence. The reason why is that the amplitude T is equal to the birefringence-induced ellipticity δ , at least for plane waves probes [12]. Once one has the flip probability then, for probes with a well-defined polarisation, the number of photons detected with orthogonal polarisation due to ‘birefringence’ is given by convolution of the probability with an incoming photon distribution.

The integral (1) or (4) in a given $f_{\mu\nu}$ is evaluated as follows. Pick a momentum l_μ , and path x^μ for the photon. Parameterise the path with nx , such that $n^2 = 0$ and $nl \neq 0$. The two independent polarisation vectors of the photon can be taken in any gauge. The integral can then be calculated. To proceed, we need a pulse model.

The most common description of focused laser fields is a Gaussian beam in the paraxial approximation. Fol-

lowing [36, 37], the paraxial beam can be defined by a wavelength λ and focal waist w_0 . These give the Rayleigh range $z_0 = \pi w_0^2/\lambda$, and the beam divergence θ_0 which we express as $s := \tan \theta_0 = w_0/z_0$. Defining $\zeta := 1/(1 + iz/z_0)$, the only nonzero field components are $B^y = E^x$, where

$$E_{\text{parax}}^x = \text{Re } E_0 e^{-i\omega(t-z)} \zeta e^{-\zeta \frac{r^2}{w_0^2}}, \quad (18)$$

and E_0 is the peak field strength, related to the cycle-averaged power by $P = \frac{\pi}{4} E_0^2 w_0^2$. The beam solves Maxwell’s equations up to terms of $\mathcal{O}(s)$, as is made more explicit by measuring transverse position in units of w_0 , writing $\rho := r/w_0$, and both longitudinal position and time in units of z_0 , writing $z = z_0 \hat{z}$, $t = z_0 \hat{t}$. Then

$$E_{\text{parax}}^x = \text{Re } E_0 e^{-i \frac{2}{s^2} (\hat{t} - \hat{z})} \zeta e^{-\zeta \rho^2}. \quad (19)$$

The first exponential is rapidly oscillating since $s \ll 1$. The second exponential is independent of s and is slowly varying in comparison. The terms neglected in the paraxial approximation are $\mathcal{O}(s)$.

Though the paraxial beam is easily understood, it is an unsatisfactory model. First, because it cannot describe a pulse: at any given point in space the field oscillates in time forever, without losing amplitude. Second, the energy in the beam is infinite⁴. The periodicity may not appear to be an issue, because our probe travels at c and quickly passes into spatial volumes where the field is damped. However, as we will show explicitly, it is in fact essential to account for pulse duration. The simplest way to do so is to add to (18) a Gaussian envelope in $t - z$ (it is not enough to add an envelope in t) as so:

$$E_{\text{pulse}}^x = \text{Re } E_0 e^{-\frac{\Delta\omega^2}{4}(t-z)^2} e^{-i\omega(t-z)} \zeta e^{-\zeta \frac{r^2}{w_0^2}}, \quad (20)$$

in which $\Delta\omega$ is a frequency spread related to the FWHM duration of the pulse, τ_L , by $\tau_L = \sqrt{8 \log 2}/\Delta\omega$. The first advantage of this ‘paraxial pulse’ over the paraxial beam (18) is that it is genuinely pulsed; the field is damped in all spacetime directions. The second advantage is that the pulse energy \mathcal{E} ,

$$\mathcal{E} = \frac{1}{2} \int d^3\mathbf{x} (\mathbf{E}^2 + \mathbf{B}^2), \quad (21)$$

is finite. Plugging (20) into this expression and integrating out r leaves, changing variable $\hat{z} \rightarrow u = (\hat{z} - \hat{t})/s^2$,

$$\mathcal{E} = \frac{\pi E_0^2 w_0^2}{2\omega} \int du e^{-\frac{2\Delta\omega^2}{\omega^2} u^2} \left[1 + \frac{C + (s^2 u + \hat{t})S}{1 + (s^2 u + \hat{t})^2} \right], \quad (22)$$

in which $C = \cos 4u$ and $S = \sin 4u$. The trig terms will be rapidly oscillating compared to the Gaussian (i.e. the

⁴ It is sometimes stated that paraxial beams have finite energy; this is a misnomer, referring only to a finite energy density obtained after integrating over transverse r .

TABLE I. Optical laser parameters proposed for the HIBEF vacuum birefringence experiment [11].

| | | | |
|----------------------|--------------------|--------------------|------------------|
| Wavelength λ | 800 nm | Frequency ω | 1.55 eV |
| Waist w_0 | 1.75 μm | Rayleigh z_0 | 12 μm |
| Total energy | 30 J | Power | 1 PW |

envelope will belong to the slowly varying part of the field) provided the spectral width obeys $\Delta\omega^2/\omega^2 \ll 1$. We can then apply a slowly varying phase (SVP) approximation to the integral (22), killing the trig functions and with them the time-dependent terms, leaving

$$\mathcal{E} \simeq \frac{\pi^{3/2}}{\sqrt{8}} \frac{E_0^2 w_0^2}{\Delta\omega}. \quad (23)$$

This is (within our approximation) constant, as the energy should be in a solution of Maxwell's equations. The limit $\Delta\omega \rightarrow 0$ ($\tau_L \rightarrow \infty$) recovers the infinite energy of the paraxial beam. (The same result could be obtained starting with the energy density in (21) and applying the SVP to a cycle-average over time t before computing the integrals. While averaging is somewhat natural in periodic fields, the SVP can be applied more generally.)

The paraxial pulse (20) can, unlike the beam (18), consistently account for the parameters of the proposed HIBEF vacuum birefringence experiment, see Table I [9, 11]. Expressing the energy in terms of power P as $\mathcal{E} = \tau_L P \sqrt{\pi/\log 16}$, and taking power, frequency and waist from Table I identifies $E_0 \simeq 2.99 \times 10^{-4} E_S$. Given that the total energy is 30 J, we then find the FWHM pulse duration to be $\tau_L = 28.18$ fs, essentially the expected value. These parameters are used in the following calculations. Note that $\Delta\omega/\omega \simeq 0.04$, justifying the use of the SVP. The intensity distributions of the paraxial pulse and beam are shown in Fig. 1.

The model (20) is not an exact solution to Maxwell's equations. We show though in Appendix A that all our results hold for more sophisticated models which are exact solutions. Thus the fine details of the model (e.g. higher orders in s) do not impact on our results. We therefore use here the simple model (20), both for intuition and in order to provide some analytic results.

A. Transverse impact parameter

In a birefringence experiment, the probe and target beams would be ideally aligned so that their focal spots overlap. Here we will illustrate the effect of impact parameters by considering a probe photon which reaches the focal plane of the Gaussian, $z = 0$, at the instant of peak field, $t = 0$, but misses the focal spot (centred at the origin) by a transverse distance; this is the impact parameter r . Given the intensity distribution of our fields, we might expect that T will fall as a Gaussian $\exp -2(r/w_0)^2$.

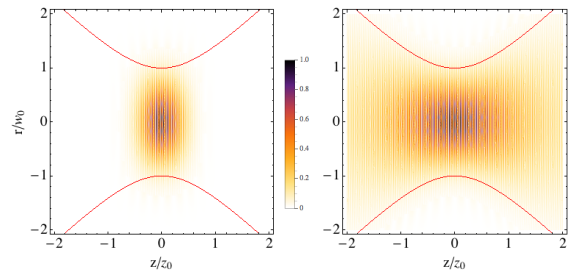


FIG. 1. Intensity distributions at $t = 0$, normalised to peak intensity. Left: the paraxial pulse (20). Right: the paraxial beam (18), for which the intensity is periodic in time.

We let the photon travel down the z -axis, so that $l^\mu = \omega'(1, 0, 0, -1)$, and we parameterise with $\phi = nx$, $n^\mu = (1, 0, 0, 1)$. The path is

$$x^\mu(\phi) = \{\phi/2, r \cos \theta, r \sin \theta, -\phi/2\}. \quad (24)$$

Taking a 45° angle between the background and probe polarisations kills the second term in (4) [6]. The resulting line integral is easily performed numerically and the results are plotted in Fig. 2.

We begin with the paraxial beam. Applying the SVP at the level of the worldline integral gives the following accurate approximation for the scattering amplitude T ,

$$T(\rho) \stackrel{\text{parax}}{\simeq} \frac{\alpha}{15} \frac{E_0^2}{E_S^2} \frac{1}{s^2} \frac{\omega'}{\omega} e^{-\rho^2} I_0(\rho^2), \quad (25)$$

with $\rho := r/w_0$ and I_0 the standard modified Bessel function. The resulting curve is indistinguishable from the numerically exact dashed curve in Fig. 2 at the scale shown⁵. The amplitude falls off if the impact factor is greater than the beam waist, $r > w_0$. This is natural given the spatial limits of the intensity distribution, see Fig. 1, but the falloff is much slower than might be expected; the Bessel function precisely cancels the exponential decrease leaving only a power law tail $\sim 1/\rho$,

$$T(\rho) \stackrel{\rho \gg 1}{\simeq} \frac{\alpha}{15} \frac{E_0^2}{E_S^2} \frac{1}{s^2} \frac{\omega'}{\omega} \frac{1}{\sqrt{2\pi\rho}}. \quad (26)$$

This would be a positive result, as such peripheral contributions could enhance e.g. birefringence signals. Unfortunately, it is unphysical, as we now show.

Assuming $\nu_0^2 := (s^2\omega/4\Delta\omega)^2 \ll 1$ (as holds for the HIBEF parameters where $\nu_0^2 \simeq 0.02$) the scattering amplitude $T(\rho)$ in a pulse is approximately given by

$$T(\rho) \stackrel{\text{pulse}}{\simeq} \frac{\alpha}{15} \frac{1}{E_S^2} \frac{\mathcal{E}\omega'}{\pi^2 w_0^2} e^{-2\rho^2}. \quad (27)$$

⁵ We emphasise that because of our polarisation choices, T is real and related to the probability by $T = \sqrt{\mathbb{P}}$, so that it is meaningful to talk about the value of the amplitude.

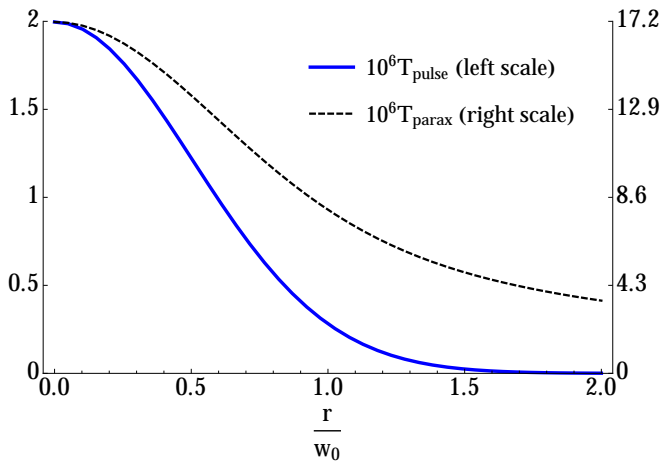


FIG. 2. The scattering amplitude T as a function of transverse impact parameter, $r/w_0 = \rho$. Parameters as in Table I. Note the different scales. The paraxial beam gives an order-of-magnitude overestimate and an unphysical enhancement at large r . (The approximations (25) and (27) are indistinguishable from the exact results on the scale shown.)

To see what this formula implies, consider Fig. 2. We first observe that, for the same parameters aside from pulse duration, the paraxial beam overestimates the amplitude by an order of magnitude (see also [38]). The reason is that, at fixed power, the paraxial beam is the ‘long pulse limit’ of the pulse, $\tau_L \rightarrow \infty$ ($\Delta\omega \rightarrow 0$), but *only* under the assumption that the pulse energy is allowed to increase to infinity. This is unphysical, but is what is implicitly assumed when using the paraxial beam.

Even if one tries to compensate by artificially reducing the field strength, we see directly from Fig. 2 that the behaviours of the amplitudes are still very different; (27), in contrast to (26), does have an exponential tail, with the same Gaussian fall-off as the intensity distribution. If we rewrite (27) in terms of peak field strength,

$$T(\rho) \stackrel{\text{pulse}}{\simeq} \frac{\alpha}{15} \frac{E_0^2}{E_S^2} \frac{1}{\sqrt{8\pi}} \frac{\omega'}{\Delta\omega} e^{-2\rho^2}, \quad (28)$$

then it is easy to compare the large impact parameter behaviour of $T(\rho)$ in the paraxial beam and pulse; asymptotically one finds

$$\frac{T_{\text{pulse}}}{T_{\text{parax}}} \xrightarrow{\rho \gg 1} 2\nu_0 \rho \exp(-2\rho^2). \quad (29)$$

At large impact parameter ρ , the amplitude in a pulse is exponentially suppressed compared to that in a paraxial beam, and the ‘enhanced signal’ seen above is lost.

More physically one can imagine, at fixed energy, compressing/stretching the pulse to increase/reduce the peak amplitude. Provided the pulse remains short, and (27) applies, such variations give a minimal effect, since we see immediately from (27) that $T(\rho) \sim \mathcal{E}$, fixed. In such a situation, and as predicted in [12], it is the total energy of the pulse which is relevant to helicity flip and birefringence.

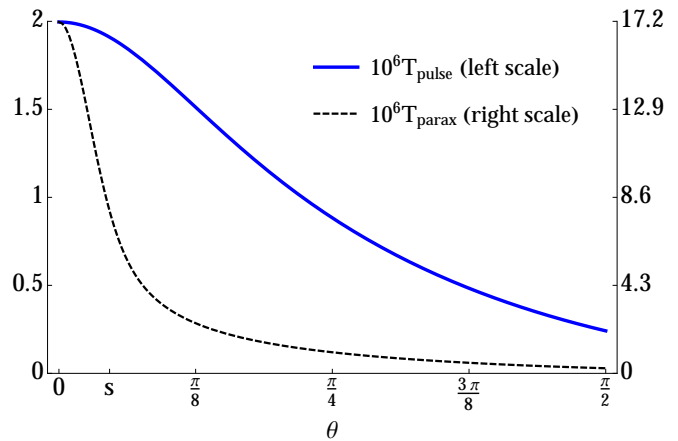


FIG. 3. The scattering amplitude T as a function of incidence angle θ . Parameters as in Table I. Note the different scales. The paraxial (black/dashed) overestimates the signal. However, T is much less sensitive to incidence angle in a pulse (solid/blue) than in the paraxial beam.

B. Angle of incidence

As a second example, consider a collision with an acute incidence angle θ between the probe and beam axes (where $\theta = 0$ is head-on). We again take the best case scenario regarding polarisations, such that the second term in (4) vanishes. The results are plotted in Fig. 3 and we see immediately that, unlike the case of impact parameter, the amplitude is much *less* sensitive to collision angle once pulse duration is accounted for.

In the paraxial beam, the amplitude drops quickly when the collision angle exceeds the beam divergence, $\theta > \tan^{-1} s \simeq s$, which again is natural. (As a function of $s^{-1} \tan \theta \sim \theta/s$ rather than r/w_0 , the curve is almost exactly the same as that for impact parameter in the beam case, Fig. 2.) In the pulse, though, the signal drops much slower, extending all the way to transverse collision angle $\theta = \pi/2$. The reason is that, while the paraxial beam is effectively a time-independent distribution, vanishing outside a spatial region, the pulse effectively exists only at the origin at a single instant, and is otherwise gone. This means that, provided the probe arrives at the origin at the right instant in time, the angle of incidence is relatively unimportant and a small deviation from a head-on collision will not significantly reduce the amplitude. This insensitivity to incidence angle is a positive result, as it indicates a certain robustness of the amplitude. It does though raise the question of what happens when the pulse arrives early or late to the focal spot, missing the instant of peak field strength.

C. Timing jitter and competing effects

Finally, we can (somewhat roughly) model the impact of ‘timing jitter’ (in e.g. triggering laser pulses) by con-

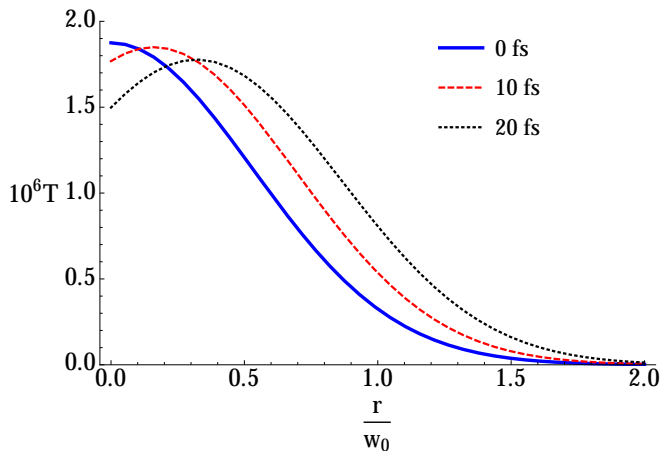


FIG. 4. The probe arrives at the focal plane $\{0, 10, 20\}$ fs after the field has peaked, with incidence angle 10° and azimuthal angle 180° . Introducing a nonzero impact parameter then improves the signal.

sidering a probe which misses the focal spot in time, as well as in space. Jitter alone naturally reduces the amplitude, as does a combination of jitter and nonzero impact parameter; if at $t = 0$ the photon is not at $z = 0$ but $z = 2z_0\tau$ and $r = w_0\rho$ then

$$T(\rho, \tau) \simeq \frac{T(0, 0)}{1 + \tau^2} e^{-2\rho^2/(1+\tau^2)}. \quad (30)$$

If multiple sources of signal reduction are known to be present, though, introducing another can actually improve the signal. Assume for example that a collision angle of 10° is required experimentally, and that a timing issue results in the probe arriving late to the focal spot. Under such conditions, deliberately introducing e.g. an impact parameter can increase the amplitude, as is shown by the dashed and dotted curves in Fig. 4. If σ is the angle between \mathbf{x}_0^\perp and \mathbf{l}^\perp , then the approximate behaviour of the amplitude is given by (30) with ρ^2 replaced by

$$\rho^2 - 2\rho\tau\theta/s \cos(\sigma) + (\tau\theta/s)^2, \quad (31)$$

which, depending on parameter values and signs, can describe a shift of the Gaussian as seen in Fig. 4.

IV. CONCLUSIONS

We have found a simple expression for the low energy photon helicity/polarisation flip probabilities in arbitrary background fields. The result can be deduced from that in a plane wave background, by observing that the light-front time integral therein can be interpreted as an integral over the worldline of a massless particle. This is another example of how lightfront field theory is well suited to studying strong field QED [39, 40]. A derivation from Heisenberg-Euler, although more involved, gives insight into the approximations behind the result, and how the

energy scales in play relate to the relevance of forward vs. back-scattering in laser-laser collisions.

The flip probability is closely related to the ellipticity to be measured in the proposed vacuum birefringence experiment at HIBEF [6, 11]. Our results therefore give us a simple method for investigating the impact of beam geometry on birefringence signals. We have seen that beam models which do not account for pulse duration (such as standard paraxial Gaussian beams) overestimate both the flip amplitude (by an order of magnitude) and the relevance of peripheral collisions. In short pulses, the signal reduction due to ‘imperfect’ collision angle is much less severe than predicted by the paraxial beam model, provided the probe is timed to arrive at the focus at close to the instant of peak field strength. While the effect of any single imperfection (collision angle, impact parameter, jitter) naturally reduces the signal, we have also seen that if it is experimentally necessary to include e.g. an angle, then it may be possible to optimise other parameters to partially counter its negative effect.

In future work, the geometry of the probe should be accounted for. The simplest way to extend from photons to beam-like probes is to take the single-photon probability (16) and integrate over an initial momentum distribution to obtain the number of produced photons with flipped polarisation. More carefully, one should go back and recalculate the probability for beam-like rather than single-photon states.

Acknowledgements

The authors are supported by the Swedish Research Council, contracts 2011-4221 (A.I. and G.T.), 2010-3727 and 2012-5644 (M.M.), and by the European Science Foundation framework *Super-Intense Laser-Matter Interactions*, grant 6481 (A.I.). A. I. thanks V. Florescu, M. Boca and the Dept. Physics, Bucharest-Măgurele for hospitality. T.H. thanks H.P. Schlenvoigt for pointing out the relevance of timing jitter.

Appendix A: Exact solutions

We confirm here that the above results hold in more sophisticated pulse models which are, in particular, exact solutions of Maxwell’s equations. We base our analysis on the Narozhny-Fofanov beam [41] (see also [42]), describing the background optical laser as a momentum distribution peaked around $k^\mu = \omega(1, 0, 0, 1)$, for propagation in the z -direction. To describe a pulse we take a distribution $\Psi(\mathbf{k})$ in $|\mathbf{k}| \in \mathbb{R}^+$, and to describe focussing we take a vectorial distribution $\Phi(\mathbf{n})$ on the photons’ direction $\mathbf{n} \in \mathbb{S}^2$. A gauge potential (in radiation gauge, $A^0 = 0 = \partial^i A^i$) is

$$\mathbf{A}(x) = \mathcal{A} \text{Re} \int d^3k \Psi(\omega) \Phi(\mathbf{n}) e^{-ikx}, \quad (A1)$$

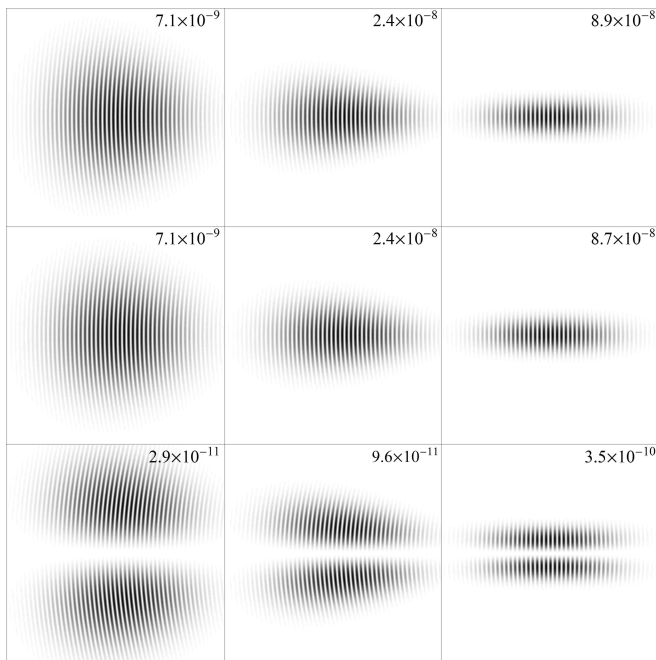


FIG. 5. E_x^2/E_S^2 (peak values shown in each panel) for the Gaussian pulse (20) (first row) and the exact solution (A1)-(A3) (second row). The third row shows longitudinal E_z^2/E_S^2 of the exact solution. The cross section is made through the x - z plane, where E_z is largest. The three snapshots are taken at 66 fs/ $20 \mu\text{m}$ apart, the rightmost being at the focus.

in which \mathcal{A} is an amplitude, $k^2 = 0$ and $\mathbf{n} = \mathbf{k}/|\mathbf{k}| = \{\sin \theta \cos \phi, \sin \theta \sin \phi, \cos \theta\}$. In [41], Ψ was chosen to be a delta function in $|\mathbf{k}|$, giving a single frequency component to the beam, and the angular distribution in Φ was limited by a step function, i.e. a ‘hard cutoff’.

We will choose a space fixed angular distribution, so that we can eliminate \mathbf{E}_y from the outset, giving linear (x) polarisation of the electric field in the plane transverse to propagation. This is analogous to the Gaussian pulse above, and mirrors the function of a real polariser. The price we pay is that the electric field will develop a longitudinal component \mathbf{E}_z , unlike in [41] where it can be taken purely transverse. When the angular spread is small, so is \mathbf{E}_z , matching what happens in a Gaussian beam when $\mathcal{O}(s)$ corrections are included. To avoid any edge effects, we take bump-function like distributions in frequency and angle which, for the focussing parameters we consider, are very close to Gaussian distributions. Explicitly, we have

$$\Psi(|\mathbf{k}|) = \exp \left[- \left(\frac{2\omega}{\pi\sigma_\omega} \right)^2 \tan^2 \left(\frac{\pi(|\mathbf{k}| - \omega)}{2\omega} \right) \right] \quad (\text{A2})$$

with $|\mathbf{k}| \in [0, 2\omega]$, and

$$\Phi(\mathbf{n}) = \exp \left(- \frac{\tan^2 \theta}{\sigma_\theta^2} \right) \hat{\mathbf{y}} \times \mathbf{n}(\theta, \phi), \quad (\text{A3})$$

where $\hat{\mathbf{y}}$ denotes the unit vector in the y -direction. The larger σ_θ , the more focused the beam and the smaller the focal waist. To parallel the discussion above, we choose $\sigma_\theta = s$ and $\sigma_\omega = \Delta\omega$. Taking the total energy to be 30J then determines the amplitude \mathcal{A} .

Though it is not possible to perform all the integrals in (A1) analytically, this exact solution of Maxwell’s equations looks very similar to (20) in position space, as shown in Fig. 5. Far from the focus the wavefronts are circular, centred at the focus. The transverse field has cylindrical symmetry around z , while the small longitudinal field is proportional to $\cos \phi$. However, the ϕ -dependent effects introduced are $\mathcal{O}(1\%)$, and we do not show them here.

In Figs 6–8 we plot T as a function of various parameters, with parameters as above. The results are practically identical to those obtained for Gaussian pulses, both in amplitude and form. Thus suggests that the results discussed here are insensitive to the fine details of the pulse model.

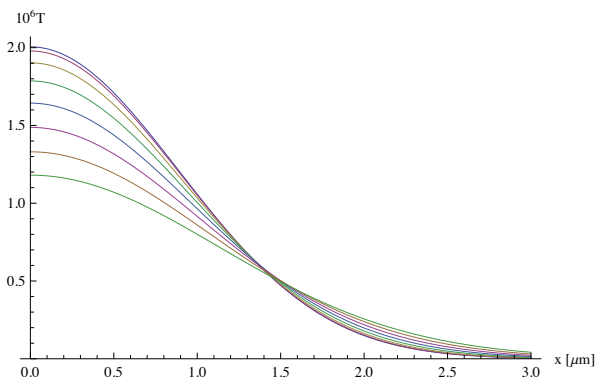


FIG. 6. The scattering amplitude T for a probe with momentum anti-parallel to z , which passes through the focal plane at time t , at a distance x from the focus. Top to bottom, $t = \{0, 10, 20 \dots 70\}$ fs.

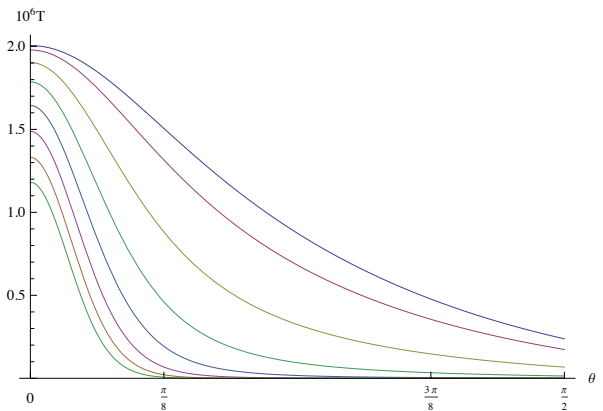


FIG. 7. The scattering amplitude T for a probe with incidence angle θ to the z -axis, which passes through the focus at (top to bottom) times $t = \{0, 10, 20 \dots 70\}$ fs.

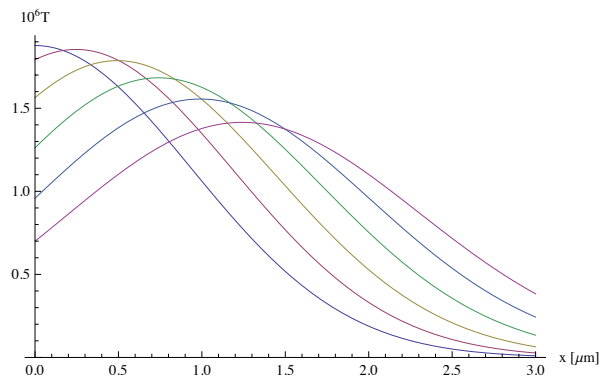


FIG. 8. The probe arrives at the focal plane a distance x from the focal point, at $\{0, 10 \dots 50\}$ fs after the field has peaked, with incidence angle 10° and azimuthal angle 180° . As in Fig. 4, a nonzero impact parameter improves the signal.

-
- [1] O. Halpern, Phys. Rev. **44**, 855 (1934).
[2] H. Euler and B. Kockel, Naturwiss. **23**, 246 (1935).
[3] W. Heisenberg and H. Euler, Z. Phys. **98**, 714 (1936) [physics/0605038].
[4] M. Marklund and P. K. Shukla, Rev. Mod. Phys. **78** (2006) 591 [hep-ph/0602123].
[5] J.S. Toll, PhD thesis, Princeton, 1952 (unpublished).
[6] T. Heinzl, B. Liesfeld, K. -U. Amthor, H. Schwöerer, R. Sauerbrey and A. Wipf, Opt. Commun. **267**, 318 (2006) [hep-ph/0601076].
[7] G. Zavattini, U. Gastaldi, R. Pengo, G. Ruoso, F. Della Valle and E. Milotti, Int. J. Mod. Phys. A **27**, 1260017 (2012) [arXiv:1201.2309 [hep-ex]].
[8] A. Cadène, P. Berceau, M. Fouché, R. Battesti and C. Rizzo, Eur. Phys. J. D **68** (2014) 16 [arXiv:1302.5389 [physics.optics]].
[9] HIBEF: <http://www.hzdr.de/db/Cms?pNid=427&pOid=35325>
[10] ELI-NP: <http://www.eli-np.ro/>
[11] H.-P. Schlenvoigt, T. E. Cowan, T. Heinzl, R. Sauerbrey, U. Schramm, *to appear*.
[12] V. Dinu, T. Heinzl, A. Ilderton, M. Marklund and G. Torgrimsson, arXiv:1312.6419 [hep-ph].
[13] G. Jarlskog, L. Joensuu, S. Pruenster, H. D. Schulz, H. J. Willutzki and G. G. Winter, Phys. Rev. D **8** (1973) 3813.
[14] M. Schumacher, I. Borchert, F. Smend and P. Rullhusen, Phys. Lett. B **59** (1975) 134.
[15] D. Bernard *et al.*, Eur. Phys. J. D **10** (2000) 141 [arXiv:1007.0104 [physics.optics]].
[16] J. M. Davila, C. Schubert and M. A. Trejo, arXiv:1310.8410 [hep-ph].
[17] R. Mohammadi, I. Motie, S.-. Xue, arXiv:1402.5999 [physics.optics].
[18] S. J. Brodsky, H. -C. Pauli and S. S. Pinsky, Phys. Rept. **301** (1998) 299 [hep-ph/9705477].
[19] T. Heinzl, Lect. Notes Phys. **572** (2001) 55 [hep-th/0008096].
[20] G. M. Shore, Nucl. Phys. B **778**, 219 (2007) [hep-th/0701185].
[21] V. Bargmann, L. Michel and V. L. Telegdi, Phys. Rev. Lett. **2** (1959) 435.
[22] C. Itzykson and J. B. Zuber, “*Quantum Field Theory*”, McGraw-Hill, New York, International Series In Pure and Applied Physics (1980).
[23] J. Zinn-Justin, “*Path Integrals in Quantum Mechanics*”, Oxford Graduate Texts, Oxford University Press (2010).
[24] N.B. Narozhnyi, Zh. Eksp. Teor. Fiz. **55**, 714 (1968) [Sov. Phys. JETP **28**, (1969)].
[25] W. Becker and H. Mitter, J. Phys. A **8**, 1638 (1975).
[26] V. N. Baier, A. I. Milshtein and V. M. Strakhovenko, Zh. Eksp. Teor. Fiz. **69**, 1893 (1975).
[27] S. Meuren, C. H. Keitel and A. Di Piazza, Phys. Rev. D **88**, 013007 (2013) [arXiv:1304.7672 [hep-ph]].
[28] F. Karbstein, arXiv:1308.6184 [hep-th].
[29] A. Di Piazza, Annals Phys. **338** (2013) 302 [arXiv:1303.5353 [hep-ph]].
[30] W. Dittrich and H. Gies, Springer Tracts Mod. Phys. **166** (2000) 1.
[31] D. R. Yennie, S. C. Frautschi and H. Suura, Annals Phys. **13** (1961) 379.
[32] W. Dittrich, Phys. Rev. D **6** (1972) 2094.
[33] H. Gies, F. Karbstein and N. Seegert, New J. Phys. **15**, 083002 (2013) [arXiv:1305.2320 [hep-ph]].
[34] F. Ehlötzky, K. Krajewska, and J.Z. Kaminski, Rep. Prog. Phys. **72** (2009) 046401.
[35] A. Di Piazza, C. Müller, K. Z. Hatsagortsyan and C. H. Keitel, Rev. Mod. Phys. **84** (2012) 1177 [arXiv:1111.3886 [hep-ph]].
[36] L. W. Davis, Phys. Rev. A **19**, 1177 (1979).
[37] K. T. McDonald, *Gaussian laser beams and particle acceleration* (1995), available at www.hep.princeton.edu/~mcdonald/accel/gaussian.pdf
[38] A. Di Piazza, K. Z. Hatsagortsyan and C. H. Keitel, Phys. Rev. Lett. **97** (2006) 083603 [hep-ph/0602039].
[39] R. A. Neville and F. Rohrlich, Phys. Rev. D **3** (1971) 1692.
[40] B. L. G. Bakker *et al.*, arXiv:1309.6333 [hep-ph].
[41] N. B. Narozhnyi, M. S. Fofanov, JETP **117**, 867 (2000).
[42] A. M. Fedotov, Laser Physics **19**, 214 (2009).